Department of Physics and Astronomy
University of Heidelberg

Bachelor Thesis in Physics
submitted by

Jonathan Klos

born in Wiesbaden (Germany)

2018

Examining Numerical Accuracy of Cosmological Simulations based on the Schrödinger-Poisson System

This Bachelor Thesis has been carried out by Jonathan Klos at the
Institute for Theoretical Physics in Heidelberg
under the supervision of
Prof. Dr. Luca Amendola
and
Prof. Dr. Sandro Wimberger

Abstract

Within the topic of large scale structure formation in the early universe, numerical simulations of the temporal evolution of cold dark matter in an expanding universe remain an area of current research. The dynamics of collisionless dark matter as modelled by the Vlasov-Poisson system may be approximated by the Schrödinger-Poisson system. We investigate the numerical accuracy of a scheme that integrates this Schrödinger method in one spatial dimension using a Crank-Nicolson finite difference scheme. In particular, we focus on the non-linear growth regime and find that here, the solver suffers a significant loss of accuracy. Moreover, we investigate the use of a dynamic time step and find it capable of alleviating the loss of accuracy, though it may not be sufficient to allow the solver to resolve a full scale cosmological simulation in a sufficiently well-behaved and accurate manner.

Zusammenfassung

Auf dem Gebiet der Entstehung großskaliger Strukturen in frühen Universum sind numerische Simulationen zur zeitlichen Entwicklung kalter dunkler Materie in einem expandierenden Universum weiterhin ein Gebiet aktueller Forschung. Die Dynamik kollisionsfreier dunkler Materie, modelliert durch die Vlasov-Poisson-Gleichungen, lässt sich durch die Schrödinger-Poisson-Gleichusngen aproximieren. Wir untersuchen die numerische Genauigkeit eines Verfahrens, das diese Schrödinger-Methode in einer Raumdimension mittels eines Crank-Nicolson-Finite-Differenzen-Verfahrens integriert. Besonders konzentrieren wir uns auf das Regime nichtlinearen Wachstums und sehen, dass das Verfahren hier erheblich an Genauigkeit einbüßt. Weiterhin untersuchen wir die Nutzung eines dynamischen Zeitschrittes, welcher es zwar gelingt den Genauigkeitsverlust zu lindern, die jedoch nicht zwingend ausreichend ist, um es dem Verfahren zu gestatten, eine vollständige kosmologische Simulation auf ausreichend ordentliche und genaue Weise aufzulösen.

Contents

Chapter 1

Introducing the 1D SPS solver

The complex dynamics of the expanding universe and the matter within is often prohibitive to an analytical approach. In order to test theories and make predictions beyond perturbation theory [1], numerical simulations are therefore an important tool in cosmology. We will firstly recount the basic principles of cosmic structure formation before introducing the Schrödinger-Poisson method as a way of approximating self-gravitating, collisionless dark matter and elaborating on the Predictor-Corrector Crank-Nicolson scheme employed to integrate the Schrödinger-Poisson system in one spatial dimension.

The model we use for the numerical simulation of the formation of large-scale structures in an expanding universe is based on several simplifying assumptions. First, we assume that since dark matter greatly outweighs baryonic matter according to astronomical observations, it will dominate the process of structure formation. Thus, we model all matter as cold, dark and collisionless. Second, we split the dark matter density into a homogeneous background and an initially small perturbation from which structure will evolve:

$$\rho(t, \mathbf{r}) = \rho_m(t) \left(1 + \delta(t, \mathbf{r})\right). \tag{1.1}$$

Here we take $\rho_m(t)$ to be the average matter density

$$\rho_m(t) = \langle \rho(t, \mathbf{x}) \rangle \,, \tag{1.2}$$

which implies that

$$\langle \delta(t, \mathbf{r}) \rangle = 0. \tag{1.3}$$

For the sake of the expansion of the universe, we will ignore the perturbative part and resolve the equation of general relativity for a homogeneous, isotropic universe. Within this expanding universe, the evolution of cold, dark matter can be modelled using Newtonian mechanics since the gravitational fields involved are sufficiently weak and the velocities involved are non-relativistic [2].

1.1 The ΛCDM universe

The ΛCDM model of the expanding universe can be found using Einstein's equations in the presence of a cosmological constant Λ under the assumptions of homogeneity and isotropy. The relevant solution of Einstein's equations is the Robertson-Walker metric [6] for a spatially flat universe, where the expansion of the universe is governed by a time-dependent scale factor $a\,(t)$ which is defined such that $a = 1$ at present time and whose evolution obeys

$$H^2(t) = \left(\frac{\dot{a}}{a}\right)^2 = H_0^2 \left(\Omega_{m0} a^3 + \Omega_{\Lambda 0}\right), \tag{1.4}$$

where $H(t)$ denotes the Hubble parameter, H_0 the Hubble constant at present time, Ω_{m0} the matter density parameter and $\Omega_{\Lambda 0}$ the dark energy density parameter arising from the cosmological constant Λ.

Note that we regard the matter-dominated era of the universe for structure formation, which is why we dropped contributions from radiation.

The density parameters are defined as

$$\Omega_{m0} = \frac{\rho_{m0}}{\rho_{c0}} = \frac{8\pi G}{3H_0^2}\rho_{m0} \tag{1.5}$$

and

$$\Omega_{\Lambda 0} = \frac{\Lambda c^2}{3H_0^2}, \tag{1.6}$$

where the critical density ρ_{c0} is given by

$$\rho_{c0} = \frac{3H_0^2}{8\pi G} \tag{1.7}$$

and G is the gravitational field constant, ρ_{m0} the average matter density at present time and c the speed of light.

Observational data from the Planck Collaboration [3] places the values of the present time matter density parameter at

$$\Omega_{m0} = 0.308 \tag{1.8}$$

while $\Omega_{\Lambda 0}$ can then be computed by solving (1.4) for $a = 1$, in which case $H = H_0$ and thus

$$\Omega_{\Lambda 0} = 1 - \Omega_{m0} = 0.692. \tag{1.9}$$

Since space in a ΛCDM universe is constantly expanding, it is useful to introduce comoving coordinates when talking about distances and the positions of objects. The physical position $\mathbf{r}$ is then given by

$$\mathbf{r}(t) = a(t)\mathbf{x}(t) \tag{1.10}$$

in terms of the comoving position $\mathbf{x}(t)$.

As comoving distances do not increase with the expansion of space, the average matter density in the comoving frame will remain constant:

$$\langle \rho(t, \mathbf{x}) \rangle = \rho_m(t) = \rho_{m0}. \tag{1.11}$$

Another quantity commonly used in astronomy is the cosmological redshift z, which relates to the scale factor a as

$$z = \frac{1}{a} - 1. \tag{1.12}$$

1.2 The Vlasov-Poisson system

In the expanding universe, the motion $\dot{\mathbf{r}}$ of an object at position $\mathbf{r}$ relative to an observer at $\mathbf{r} = 0$ separates into a recession velocity due to the expansion

of space and a peculiar velocity in respect to the comoving frame:

$$\dot{\mathbf{r}} = \dot{(a\mathbf{x})} = \dot{a}\mathbf{x} + a\dot{\mathbf{x}}. \tag{1.13}$$

In the comoving frame, the expansion is factored out and only the peculiar velocity $a\dot{\mathbf{x}}$ remains.

Using this, we write down the classical Lagrangian of a dark matter particle of mass m moving in a gravitational potential $V(t, \mathbf{x})$ in the comoving frame.

$$\mathfrak{L}(\mathbf{x}, \dot{\mathbf{x}}, t) = \frac{m}{2} (a\dot{\mathbf{x}})^2 - mV(t, \mathbf{x}) \tag{1.14}$$

or, using conjugate momentum and velocity

$$m\mathbf{u} = \mathbf{p} = \frac{\partial \mathfrak{L}}{\partial \dot{\mathbf{x}}} = ma^2\dot{\mathbf{x}}, \tag{1.15}$$

$$\mathfrak{L}(\mathbf{x}, \mathbf{u}, t) = \frac{m}{2a^2}\mathbf{u}^2 - mV(t, \mathbf{x}). \tag{1.16}$$

Due to symmetry, the homogeneous part of the matter density does not contribute to the gravitational potential apart from a constant. This is because any contribution with non-vanishing gradient would yield a preferred direction and thus violate isotropy. Thus, the gravitational potential $V(t, \mathbf{x})$ in which the dark matter moves is defined by

$$\Delta_x V(t, \mathbf{x}) = \frac{4\pi G \rho_{m0}}{a} \delta(t, \mathbf{x}). \tag{1.17}$$

As we model dark matter as collisionless, it is clear that just monitoring the density may be insufficient to fully capture the dynamics of, for example, the gravitational collapse of a dark matter halo, where streams of dark matter with different velocities may meet.

For studying the temporal evolution of dark matter, we will thus use the phase space density $f(t, \mathbf{x}, \mathbf{u})$ which must fulfill

$$\int \mathrm{d}^3u \; f(t, \mathbf{x}, \mathbf{u}) = \frac{\rho(t, \mathbf{x})}{\rho_{m0}} = 1 + \delta(t, \mathbf{x}). \tag{1.18}$$

A classical description of collisionless matter subject to its own gravity is given by the Vlasov-Poisson system (VPS). It describes the evolution of the phase-space distribution $f(t, \mathbf{x}, \mathbf{u})$ as follows:

$$\partial_t f = -\frac{\mathbf{u}}{a^2} \cdot \nabla_x f + \nabla_x V \cdot \nabla_u f, \tag{1.19}$$

$$\Delta_x V = \frac{4\pi G \rho_{m0}}{a} \left(\int \mathrm{d}^3 u f - 1 \right). \tag{1.20}$$

As the VPS is, in essence, a collisionless Boltzmann equation in the presence of an external force defined by the potential V, it can similarly be derived as an ensemble average of an N-particle system or by starting at the phase-space trajectories and applying Liouville's theorem [7, 8].

1.3 The Schrödinger method as a VPS approximation

It was shown in [7] that the VPS may be approximated in a specific way using the so-called Schrödinger method.

We introduce the coupled Schrödinger-Poisson system (SPS) for the complex scalar field ψ.

$$i\mu \partial_t \psi(t, \mathbf{x}) = \left[-\frac{\mu}{2a^2} \Delta + V(t, \mathbf{x}) \right] \psi(t, \mathbf{x}), \tag{1.21}$$

$$\Delta V(t, \mathbf{x}) = \frac{4\pi G \rho_{m0}}{a} \left(\frac{|\psi(t, \mathbf{x})|^2}{\langle |\psi(t, \mathbf{x})|^2 \rangle} - 1 \right). \tag{1.22}$$

Here, μ is a free parameter which will determine the phase space resolution of the model. We also introduce the Husimi distribution f_H which is given as the square amplitude of the Husimi representation ψ_H of ψ.

$$f_H(t, \mathbf{x}, \mathbf{u}) = |\psi_H(t, \mathbf{x}, \mathbf{u})|^2 \tag{1.23}$$

where

$$\psi_H(t, \mathbf{x}, \mathbf{u}) = \frac{1}{(2\pi\mu)^{\frac{3}{2}}} \frac{1}{(2\pi\sigma_x^2)^{\frac{3}{4}}} \int \mathrm{d}^3 y \, \exp\left(-\frac{(\mathbf{x} - \mathbf{y})^2}{4\sigma_x^2} - \frac{i}{\mu} \mathbf{u} \cdot \mathbf{y} \right) \psi(t, \mathbf{y}). \tag{1.24}$$

It can then be shown analytically that the temporal evolution of the Husimi distribution is, up to terms of $\mathcal{O}(\mu^2)$, equivalent to a coarse-grained Vlasov-Poisson system for a phase space distribution $\bar{f}$ smoothed by a Gaussian filter as such:

$$\bar{f}(t,\mathbf{x},\mathbf{u}) = \frac{1}{(\pi\mu)^3}\int \mathrm{d}^3y\mathrm{d}^3v \exp\left(-\frac{(\mathbf{x}-\mathbf{y})^2}{2\sigma_x^2}\right)\exp\left(-\frac{2\sigma_x^2}{\mu^2}(\mathbf{u}-\mathbf{v})^2\right) f(t,\mathbf{y},\mathbf{v}). \tag{1.25}$$

We say that the Husimi distribution approximates the coarse-grained Vlasov-Poisson system in the following way:

$$\partial_t\left(\bar{f} - f_H\right) = \mathcal{O}(\mu^2). \tag{1.26}$$

A full analytical proof of this Husimi-Vlasov correspondence may be found in [7] and a numerical study in two spatial dimensions in [4]

1.4 The PC-CNFD Schrödinger-Poisson Solver for 1D

We will now introduce the Predictor-Corrector Crank-Nicolson solver developed in [8] which integrates the SPS in one spatial and one temporal dimension using a Crank-Nicolson finite difference scheme.

The solver uses the following dimensionless coordinates:

$$\mathrm{d}\xi = \frac{1}{\mu^{\frac{1}{2}}}\left[\frac{3}{2}H_0^2\Omega_{m0}\right]^{\frac{1}{4}}\mathrm{d}x, \tag{1.27}$$

$$\mathrm{d}\tau = \frac{1}{a^2}\left[\frac{3}{2}H_0^2\Omega_{m0}\right]^{\frac{1}{2}}\mathrm{d}t, \tag{1.28}$$

which allow the wave function and gravitational potential to be rescaled in the following way:

$$\Psi(\tau,\xi) = \frac{\psi(\tau,\xi)}{\sqrt{\langle|\psi(\tau,\xi)|^2\rangle}}, \tag{1.29}$$

$$U(\tau,\xi) = \frac{a}{\mu}\left[\frac{3}{2}H_0^2\Omega_{m0}\right]^{-\frac{1}{2}}V(\tau,\xi). \tag{1.30}$$

We can then rewrite the Schrödinger-Poisson equations (1.21) and (1.22) for one spatial dimension in said coordinates to get a set of dimensionless equations for the rescaled Ψ and U.

$$i\partial_\tau \Psi = \left[-\frac{1}{2}\partial_\xi^2 + aU \right] \Psi, \tag{1.31}$$

$$\partial_\xi^2 U = |\Psi|^2 - 1. \tag{1.32}$$

The solver integrates these equations on a 2D space-time interval

$$[0, L] \times [0, \tau_{end}] \tag{1.33}$$

with periodic boundary conditions for the spatial dimension. Here L is the size of the spatial domain and τ_{end} the final simulation time.

On this interval, Ψ and U are evaluated on a $N \times M$ space-time mesh, giving a uniform spatial grid with N points and a uniform temporal grid with M points. An alternative way of characterizing this mesh is the spatial grid resolution $\Delta\xi$ and the time step size $\Delta\tau$.

$$\Delta\xi = \frac{L}{N},\ \Delta\tau = \frac{\tau_{end}}{M}. \tag{1.34}$$

The Laplace operator is approximated up to second order in $\Delta\xi$ using the central finite difference method:

$$\frac{\partial^2}{\partial\xi^2} F(\xi) = \frac{F(\xi - \Delta\xi) - 2F(\xi) + F(\xi + \Delta\xi)}{\Delta\xi^2} + \mathcal{O}(\Delta\xi^2). \tag{1.35}$$

The thus discretized operator takes the form of a cyclic tridiagonal $N \times N$ matrix, making it possible to solve (1.32) for U using a modified version of the Thomas algorithm for tridiagonal matrices [8].

The unitary time evolution operator is approximated using the Cayley form

$$\mathbf{U}(\tau + \Delta\tau, \tau) \simeq \left(\mathbf{1} + \mathbf{H}\frac{i\Delta\tau}{2} \right)^{-1} \left(\mathbf{1} - \mathbf{H}\frac{i\Delta\tau}{2} \right), \tag{1.36}$$

$$\mathbf{H}(\tau + \Delta\tau, \tau) = \frac{1}{\Delta\tau} \int_\tau^{\tau+\Delta\tau} \mathrm{d}\tau'\, H(\tau'), \tag{1.37}$$

which, after discretizing the Laplace operator as before, gives rise to an implicit Crank-Nicolson scheme capable of solving the SPS up to second order in $\Delta\xi$ and $\Delta\tau$.

$$\left(\mathbf{1} + \mathbf{H}\frac{i\Delta\tau}{2}\right)\Psi(\tau + \Delta\tau) = \left(\mathbf{1} - \mathbf{H}\frac{i\Delta\tau}{2}\right)\Psi(\tau), \tag{1.38}$$

where we use the approximation

$$\mathbf{H}(\tau + \Delta\tau, \tau) = -\frac{1}{2}\partial^2\xi + \frac{1}{2}\left(a(\tau)U(\tau) + a(\tau + \Delta\tau)U(\tau + \Delta\tau)\right) + \mathcal{O}(\Delta\tau^2). \tag{1.39}$$

However, instead of solving the set of nonlinear equations given by (1.38), the scheme is employed in a predictor-corrector fashion, where in a first cycle, the predictor cycle, (1.38) is solved after setting $U(\tau + \Delta\tau) = U(\tau)$ to reach a predicted wavefunction $\tilde{\Psi}(\tau + \Delta\tau)$ and a predicted potential $\tilde{U}(\tau + \Delta\tau)$ by solving (1.32). $\tilde{U}$ is used in a second cycle, the corrector cycle, where we set $U(\tau + \Delta\tau) = \tilde{U}(\tau + \Delta\tau)$. The resulting wave function is then taken to be $\Psi(\tau + \Delta\tau)$.

Avoiding the computationally expensive direct solution of (1.38) allows the solver to integrate each time step using $\mathcal{O}(N)$ operations. This gives the solver a total time complexity of $\mathcal{O}(N \cdot M)$ for a full integration of the SPS on the 2D mesh, and its accuracy can be shown to be $\mathcal{O}(\Delta\xi^2, \Delta\tau^2)$.

A scheme for the construction of cosmological initial conditions is also provided in [8]. The initial density contrast δ takes the form of a random Gaussian field which is constructed in Fourier space, where the different perturbation modes do not correlate. While the phases of the different Fourier modes are distributed uniformly, the absolute values obey a Rayleigh distribution with a frequency-specfic variance depending on the continuous matter power spectrum. The contructed cosmological initial conditions thus depend directly on L, N since these determine the contributing frequencies in Fourier space.

Chapter 2

Numerical Tests

2.1 Standard Convergence Tests

The truncation error is the accumulated error due to the numerical scheme, including approximations such as the discretization of continuous variables, functions and operations. For example, the solver we use approximates derivatives using second order finite differences. As such, contributions of $\Delta\xi^2$ and higher orders will appear in the truncation error. The truncation error is defined as the difference between the true solution of the problem and its numerical approximation in some norm. We thus introduce the discretized L_2 norm

$$||\Psi||_2 = \left(\frac{1}{N} \sum_{n=1}^{N} |\Psi(n\Delta\xi)|^2 \right)^{\frac{1}{2}} \tag{2.1}$$

to define the truncation error

$$\epsilon = ||\Psi_{true} - \Psi_{num}||_2 \tag{2.2}$$

where Ψ_{num} is the discretized wave function resulting from the numerical scheme and Ψ_{true} is the discretized solution to the SPS (1.31).

The PC-CNFD method introduced in section 1.4 is approximately $\mathcal{O}(\Delta\xi^2, \Delta\tau^2)$. Therefore, we can, for a given set of simulation parameters find constants C_ξ and C_τ so that

$$\epsilon \leq C_\xi \cdot (\Delta\xi)^2 + C_\tau \cdot (\Delta\tau)^2 \tag{2.3}$$

for all sufficiently small $\Delta\xi,\ \Delta\tau$.

Since Ψ_{true} is unknown, the truncation error ϵ can only be approximated. We do this by choosing a reference solution Ψ_{ref} computed using an appropriately fine space-time mesh and then taking

$$\epsilon_{approx} = ||\Psi_{ref} - \Psi_{num}||_2 \tag{2.4}$$

as an approximation for the true truncation error. Since

$$|\epsilon - \epsilon_{approx}| \leq ||\Psi_{true} - \Psi_{ref}||_2, \tag{2.5}$$

this approximation will naturally be more accurate the better Ψ_{ref} approximates Ψ_{true}.

For cosmological initial conditions, the approximate truncation error can only be used in a limited way. Since varying the number of points on the spatial grid also changes what frequency modes of the matter power spectrum contribute to the initial conditions, initial conditions for a finer grid do not equate to simply a finer sampling of the same initial conditions. Thus it is, as is, not easily possible to gauge the impact of the number of grid points on the numerical accuracy of the solver using this method as the reference solution Ψ_{ref} must have the same number of grid points as the numerical solution Ψ_{num} to be tested.

2.2 Layzer-Irvine Test

Another test for the numerical accuracy of the SPS solver was introduced in [4, 8]. The Layzer-Irvine test is a global energy test taking its name from the Layzer-Irvine energy equation. Since total energy is not actually conserved in the comoving, non-inertial frame in an expanding universe, it obeys a non-trivial time dependence which we will briefly outline here:

We begin by separating the total energy per mass E into kinetic and potential terms K and W:

$$E = K + W. \tag{2.6}$$

These terms can, according to (1.21), be expressed as

$$K = \int \mathrm{d}x \, \frac{\mu^2}{2a^2} |\nabla_x \psi(x,t)|^2 = C_\varepsilon \frac{1}{a^2} \int \mathrm{d}\xi \, |\nabla_\xi \Psi(\xi,\tau)|^2 \tag{2.7}$$

and

$$W = \int \mathrm{d}x \, \frac{1}{2} V(x,t) |\psi(x,t)|^2 = C_\varepsilon \frac{1}{a} \int \mathrm{d}\xi \, U(\xi,\tau) |\Psi(\xi,\tau)|^2 \tag{2.8}$$

where

$$C_\varepsilon = \frac{\mu^{\frac{3}{2}}}{2} \left\langle |\psi(\tau,\xi)|^2 \right\rangle \left[\frac{3}{2} H_0^2 \Omega_{m0} \right]^{\frac{1}{4}} \tag{2.9}$$

is a constant that results from rewriting the above expressions in dimensionless coordinates according to (1.27) and inserting the rescaled wave function and potential (1.29, 1.30).

Time derivation of the total energy per mass gives

$$\frac{\mathrm{d}E}{\mathrm{d}t} = -\frac{\dot{a}}{a}(2K + W), \tag{2.10}$$

which coincides with Layzer-Irvine energy equation for a classical homogeneous matter distribution in an expanding universe [5] due to the kinetic and potential energy terms scaling with a in the same way.

After rewriting this as $\frac{\mathrm{d}}{\mathrm{d}a}(aE) = -K$, we can define the error

$$\epsilon = \frac{\frac{\mathrm{d}}{\mathrm{d}a}(aE)}{-K} - 1 \tag{2.11}$$

which can then be computed using numerical integration and five-point stencil finite differences to $\mathcal{O}(\Delta\xi^4)$.

This Layzer-Irvine test monitors the relative error of the change in total energy due to the expansion of the universe.

2.3 Local Schrödinger Test

Since the solver is designed to integrate the SPS, it may also be viable to test whether equation (1.31) holds. This gives us a local test by computing for a given point in spacetime the difference between the left and right side

of the dimensionless Schrödinger-Poisson equation relative to the amplitude of the rescaled wave function Ψ in that point.

We define the average relative error

$$\epsilon = \left\langle \frac{|[i\partial_\tau + \frac{1}{2}\partial_\xi^2 - aU]\Psi|}{|\Psi|} \right\rangle \tag{2.12}$$

which we compute using finite differences up to $\mathcal{O}(\Delta\xi^4, \Delta\tau^4)$.

Chapter 3

Probing the Non-Linear Growth Regime

3.1 Numerical Accuracy in the Non-Linear Regime

It was shown in [8] that for cosmological initial conditions, the results of the solver are in good agreement with the predictions of perturbation theory in the linear growth regime. As structure formation takes place largely in the non-linear growth regime, we want to test whether the solver can accurately solve the SPS outside the linear growth regime. As a first test, we use simulation parameters as recommended in [8] for a simulation with cosmological initial conditions:

$$\mu = 10^{-12}\frac{\mathrm{Js}}{\mathrm{eV}},\ L = 250\mathrm{Mpc\,h^{-1}},\ N = 2^{21}. \tag{3.1}$$

For the time step, we take a base value of

$$\Delta\tau = 0.004 \tag{3.2}$$

which is decreased by a factor of two in each of the three subsequent runs. This is equivalent to doubling the number of grid points M of the temporal grid.

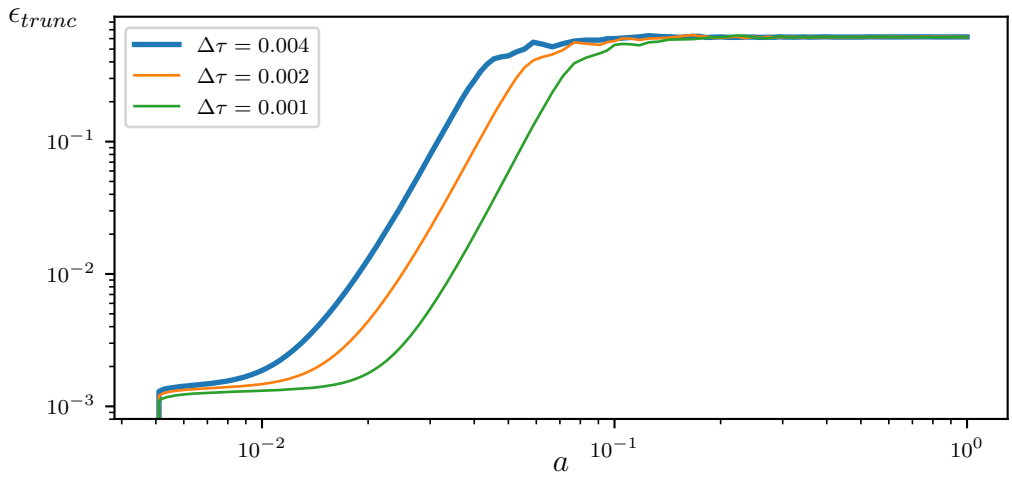

(a) Truncation error

We see from the truncation error (see Figure 3.1a) that at the onset of the non-linear regime, the solver sees a significant and rapid loss in accuracy. A smaller time step delays this, but does not seem to stop or even alleviate it. The results of the Schrödinger test agree with this observation somewhat, even if the drop in accuracy is registered at a later point in the simulation.

The Layzer-Irvine test, however, shows no loss of accuracy of this degree and the corresponding error stays below 1% throughout the entire simulation.

This suggests firstly that the solver may not converge towards the true solution in a controlled way within the non-linear regime for the chosen parameters. Secondly, it appears that the Layzer-Irvine test is not sensitive to the loss of accuracy we experience as we leave the linear growth regime, making it less useful for assessing whether our solution converges with $\Delta\xi^2$, $\Delta\tau^2$.

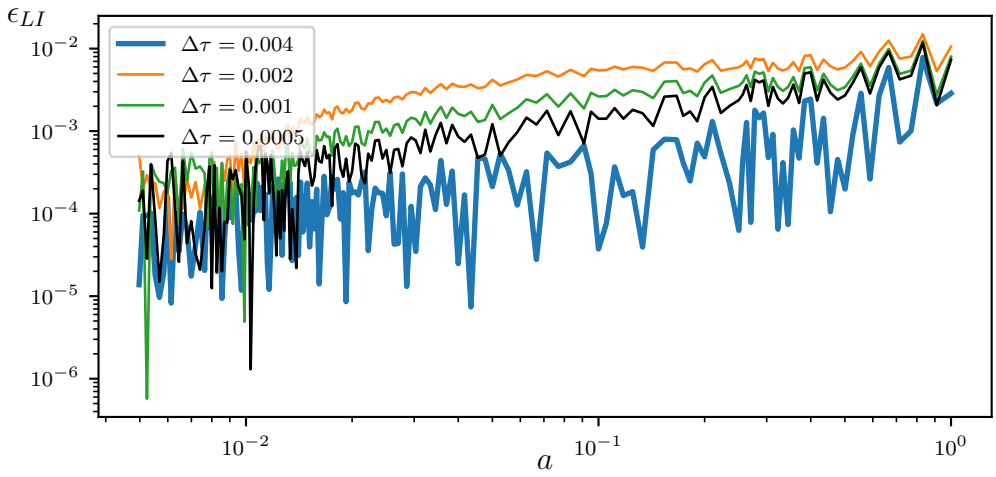

(b) Layzer-Irvine test

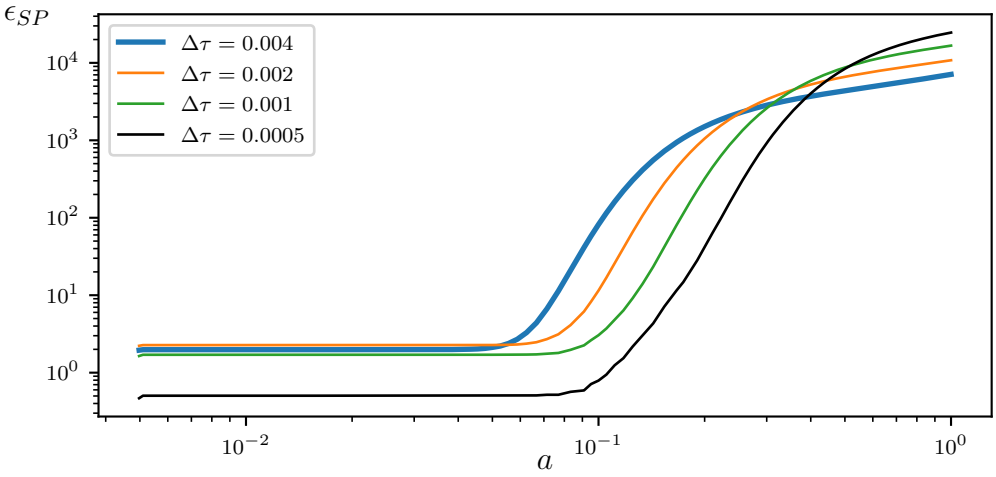

(c) Local Schrödinger test

Figure 3.1: Results for the different numerical tests introduced in chapter 2. To approximate the truncation error, the numerical solution for the smallest time step used ($\Delta\tau = 0.0005$) was used as reference wave function Ψ_{ref}. From the results of [8] we expect the linear growth regime to last until at least $z = 100$.

3.2 Testing Numerical Accuracy for fixed a

If we want to study the behaviour of the solver in the non-linear growth regime more in depth, it is prudent to remind ourselves that the non-linearity in the SPS comes from the contribution of the gravitational potential, the term aU in (1.31).

The impact of this term increases with a as the universe expands and with U as initially small perturbations in the matter distribution grow. To better understand in what way each of these affect numerical accuracy, we set the scale factor a to one fixed value a_{const} for the entirety of the simulation. This allows us to better study under which conditions the non-linear contributions may or may not affect the accuracy of the solver.

Physically, running the simulation with fixed a represents simulating a non-expanding, static universe. Numerically, it fixes the strength of the non-linear gravitational interaction, allowing us to gauge in which regimes our solver remains stable.

As increasing the point densities of the spatial and temporal grids comes with an increase in required computational resources, we will, for the sake of this thesis, not be able to provide these tests for a full-scale cosmological simulation. We take the following non-varying parameters:

$$\mu = 10^{-12}\frac{\mathrm{Js}}{\mathrm{eV}},\ L = 2.5\mathrm{Mpc\,h^{-1}}. \tag{3.3}$$

We choose a base grid size of

$$N = 2^{15} \tag{3.4}$$

and vary grid size by doubling the number of grid point for each of three consecutive finer spatial grids. Additionally, we choose a base time step of

$$\Delta\tau = 0.0008 \tag{3.5}$$

which is halved each time for the three smaller time steps.

For the constant scale factor, we choose a base value

$$a_{const} = 0.02 \tag{3.6}$$

with two higher values of a_{const} achieved by doubling this value.

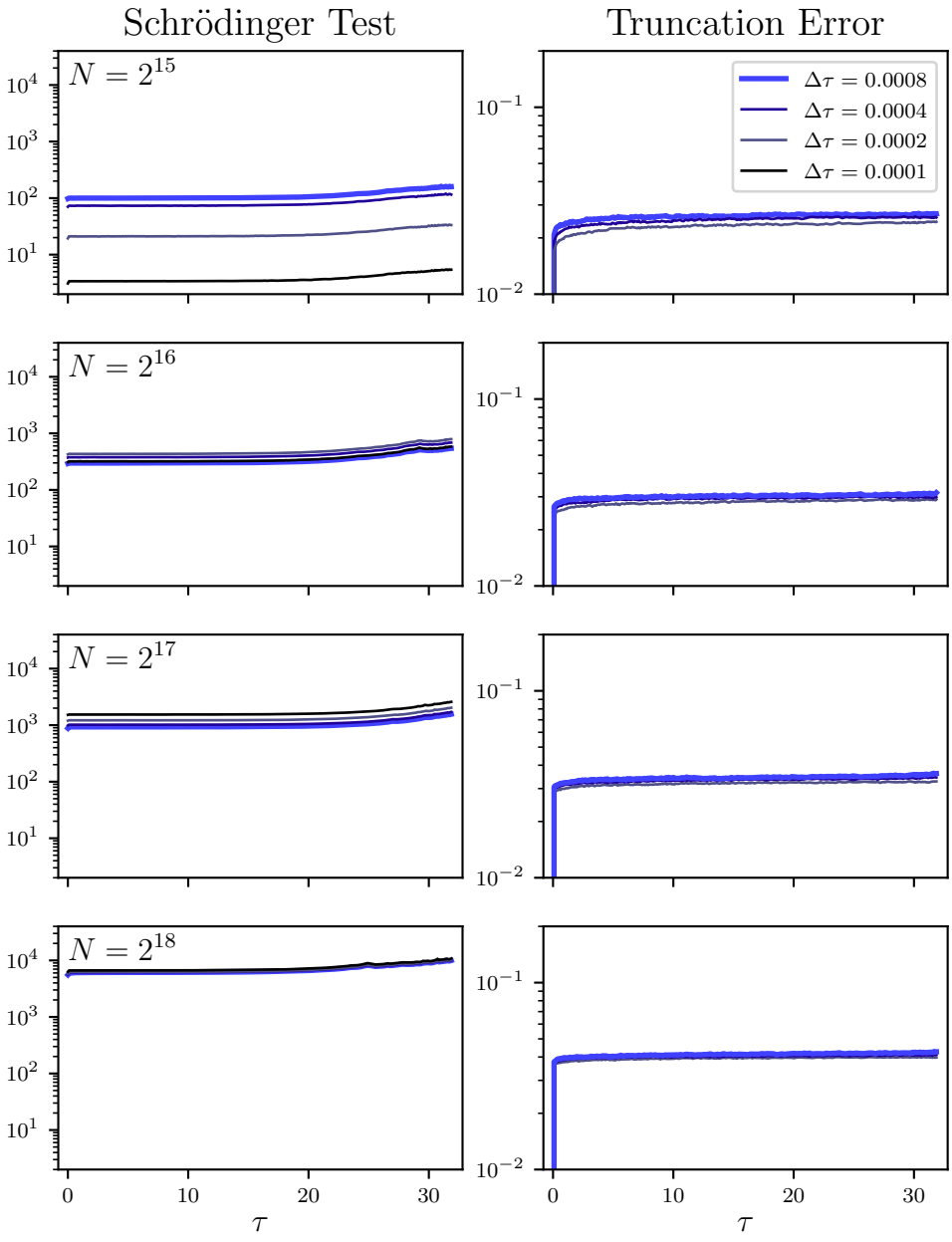
Schrödinger Test
Truncation Error
$N = 2^{15}$
$N = 2^{16}$
$N = 2^{17}$
$N = 2^{18}$
$\Delta\tau = 0.0008$
$\Delta\tau = 0.0004$
$\Delta\tau = 0.0002$
$\Delta\tau = 0.0001$
10^4
10^3
10^2
10^1
10^{-1}
10^{-2}
0
10
20
30
τ

(a) $a_{const} = 0.02$

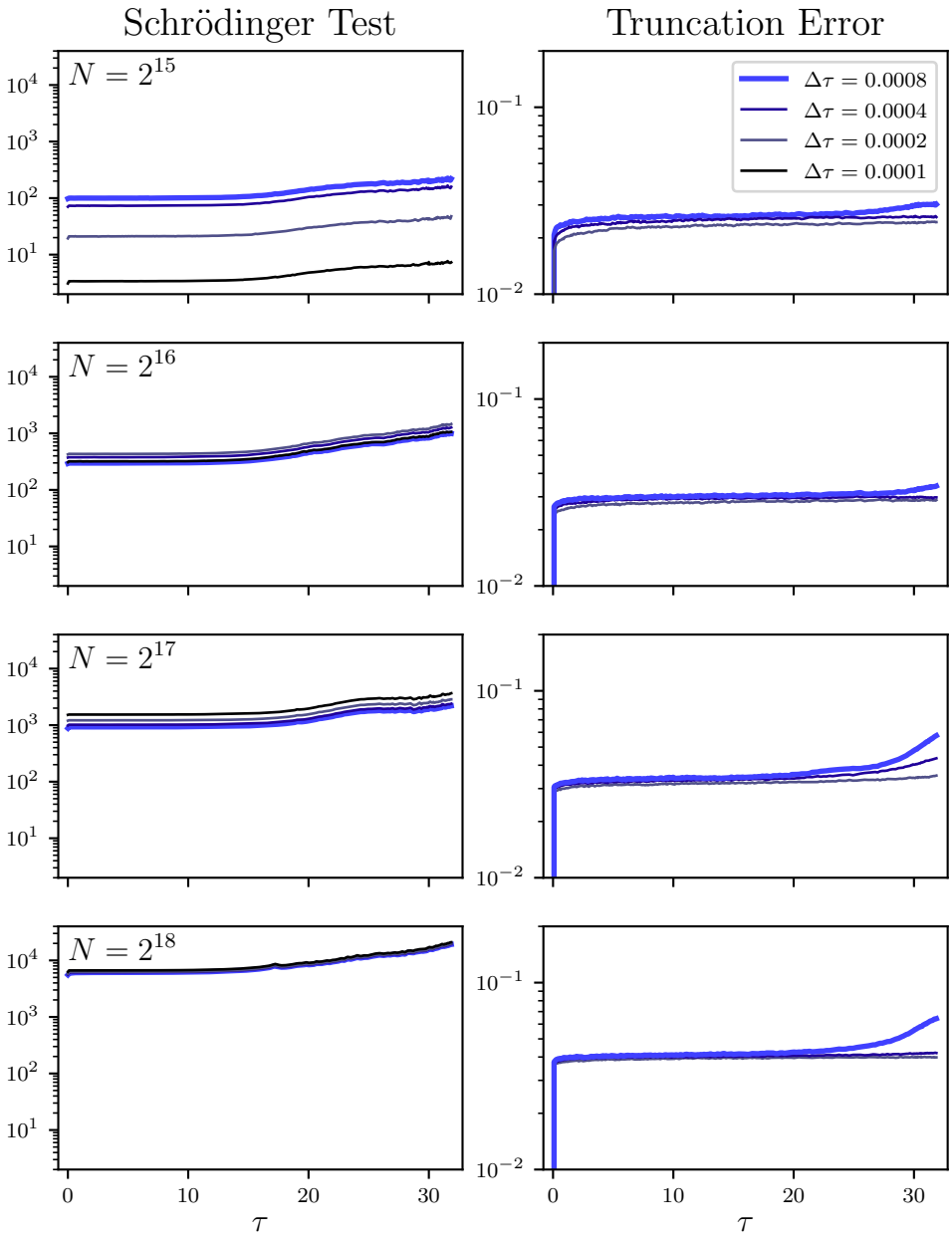
Schrödinger Test
Truncation Error
$N = 2^{15}$
$N = 2^{16}$
$N = 2^{17}$
$N = 2^{18}$
$\Delta\tau = 0.0008$
$\Delta\tau = 0.0004$
$\Delta\tau = 0.0002$
$\Delta\tau = 0.0001$
10^4
10^3
10^2
10^1
10^{-1}
10^{-2}
0
10
20
30
τ

(b) $a_{const} = 0.04$

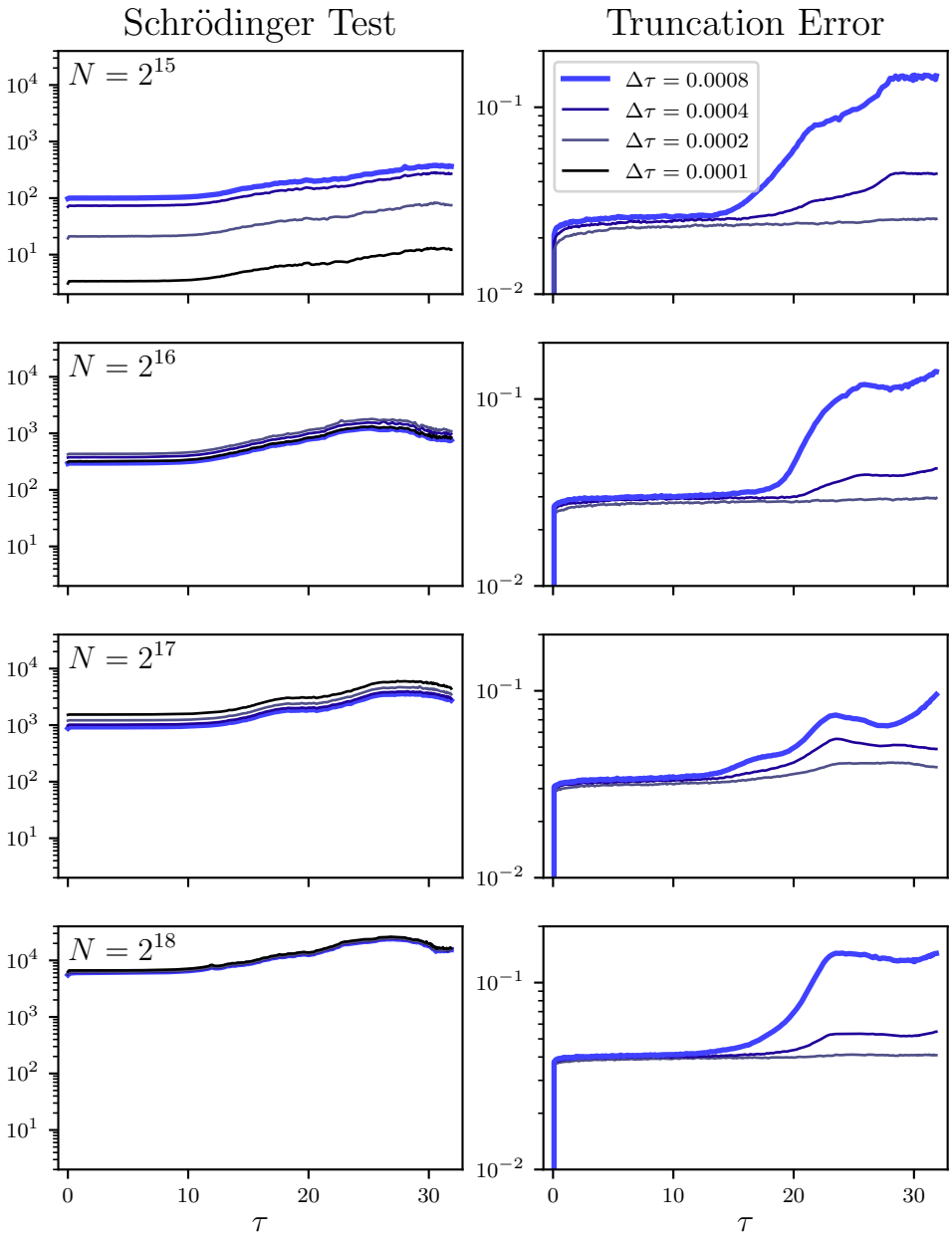

(c) $a_{const} = 0.08$

Figure 3.2: Results of the Schrödinger test and truncation error for simulation runs with different fixed scale factors a_{const}.

τ_{end} is chosen such that $[0, \tau_{end}]$ corresponds to a time frame from $z = 200$ to $z = 0$ in an expanding universe. More details on the relation between superconformal time τ and scale factor a may be found in [8].

The Layzer-Irvine test is not used here as the Layzer-Irvine equation does not apply in a static universe where a remains constant.

Of note is that the value of a_{const} has little effect on numerical accuracy at simulation start, suggesting that the main reason for loss of accuracy in the non-linear regime is, in fact, mostly due to the growth of the initial perturbations, which happens earlier and faster for larger a_{const}.

Increasing spatial resolution seems to have only limited effect under our conditions, though it may be more effective for larger domains. The effect of varying the time step seems to be more pronounced for smaller spatial grids.

Generally, for a good spatial resolution, it seems more useful to vary the time step to improve accuracy rather than to go to a finer spatial grid.

3.3 Adaptive Time Step

One way to improve the numerical accuracy of the solver suggested in [8] is the implementation of a dynamically chosen time step instead of a static time step.

We do this by introducing a coarser, uniform temporal grid to allow the synchronisation of simulations using different and varying time steps. At each step of the coarse grid, we evaluate all relevant time scales to arrive at a target time step, based upon which the refinement of the coarse grid is chosen.

Let M_0 be the number of grid points in the coarse grid. The ith step of the coarse grid corresponds to the time

$$\tau_i = i\frac{\tau_{end}}{M_0} \tag{3.7}$$

We refine the coarse grid by dividing the interval $[\tau_i, \tau_{i+1}]$ into m_i steps, where

we choose m_i such, that the dynamic time step

$$\Delta\tau_{dyn} = \frac{\tau_{i+1} - \tau_i}{m_i} \tag{3.8}$$

is close to the target time step.

We will now introduce some examples for time scales that may be used in determining such a dynamic time step.

3.3.1 The Free Fall Time Scale

We first introduce the free fall time scale, defined here as the time needed for a uniform spherical overdensity ρ_{OD} to collapse completely according to classical Newtonian mechanics (1.19).

Solving the equations of motion in one spatial dimension yields the free fall time

$$t_{freefall} = \sqrt{\frac{2}{4\pi G\rho_{OD}}} \tag{3.9}$$

which we rewrite by transforming to dimensionless coordinates and replacing the density contrast with the wave function amplitude:

$$\tau_{freefall} = \sqrt{\frac{2}{a\left(|\Psi|^2 - 1\right)}}. \tag{3.10}$$

From this we can define the free fall time step up to a parameter $C_{freefall}$

$$\Delta\tau_{freefall} = C_{freefall}\frac{1}{\sqrt{a\left(\max_\xi |\Psi|^2 - 1\right)}} \tag{3.11}$$

where $C_{freefall} \overset{!}{<} \sqrt{2}$.

We use

$$C_{freefall} = 0.002. \tag{3.12}$$

3.3.2 The Flow Time Scale

For a specific velocity u, the spatial resolution Δx gives a natural flow time scale

$$t_{flow} = \frac{\Delta x}{u}. \tag{3.13}$$

We define, within our system of dimensionless coordinates, the dimensionless velocity

$$\upsilon = \frac{1}{\mu^{\frac{1}{2}}} \left[\frac{3}{2} H_0^2 \Omega_{m0} \right]^{-\frac{1}{4}} u \tag{3.14}$$

which gives us an expression of the flow time scale in code units:

$$\tau_{flow} = \frac{\Delta\xi}{a^2 \upsilon}. \tag{3.15}$$

From the Husimi distribution, we can find that the average velocity at a given position is

$$\langle \upsilon \rangle = \partial_\xi \phi \tag{3.16}$$

where ϕ is the phase of the wave function:

$$\Psi = \sqrt{A} e^{i\phi}. \tag{3.17}$$

We can thus define the flow time step

$$\Delta\tau_{flow} = C_{flow} \frac{\Delta\xi}{a^2 \max_\xi |\partial_\xi \phi|} \tag{3.18}$$

with a free parameter $C_{flow} \overset{!}{<} 1$.

We use

$$C_{flow} = 0.5. \tag{3.19}$$

3.3.3 Constant Physical Time

Since the dimensionless superconformal time τ defined in (1.28) relates to the physical time t in a non-linear fashion, we may introduce a time scale defined such that the corresponding physical time remains constant.

We define

$$\Delta\tau_{CPT} = C_{CPT} \cdot a^{-2} \tag{3.20}$$

where C_{CPT} is a free parameter.

We use

$$C_{CPT0} = 5 \cdot 10^{-6}. \tag{3.21}$$

3.3.4 Effects on Numerical Accuracy

To gauge the effect of using a dynamic time step, we will first include a control run using a static time step of

$$\Delta\tau = 0.001. \tag{3.22}$$

The second simulation will use a dynamic time scale combining free fall time and flow time

$$\Delta\tau_{dyn} = \min\left\{\Delta\tau_{static},\ \Delta\tau_{freefall},\ \Delta\tau_{flow}\right\}, \tag{3.23}$$

while a third run will use the CPT scale

$$\Delta\tau_{dyn} = \min\left\{\Delta\tau_{static},\ \Delta\tau_{CPT}\right\}. \tag{3.24}$$

Finally, to be able to approximate the truncation error, we will use a static time step of

$$\Delta\tau = 0.000125 \tag{3.25}$$

to compute a reference wave function.

In addition, we set the following parameters for all simulations:

$$\mu = 10^{-12}\frac{\mathrm{Js}}{\mathrm{eV}},\ L = 10\mathrm{Mpc\,h^{-1}},\ N = 2^{18}. \tag{3.26}$$

As the onset of the dynamic time step for combined free fall and flow time scales happens well in the regime where the numerical solutions drift apart, it cannot prevent the increase in truncation error, though it does reduce its growth greatly once it sets in (See Figure 3.4a). The CPT scale, setting in at an earlier time, manages to suppress and delay the loss of accuracy to a greater degree, though it does not prevent it completely. Whether this is due to a growing error despite increasingly smaller time steps or due to the error in the approximation of the truncation error itself is not possible to discern at this point. In particular, the approximation of the truncation error is connected to the error of the reference wave function (2.5), which may not be sufficiently small here as $\Delta\tau_{dyn}$ becomes smaller than the time step $\Delta\tau =$

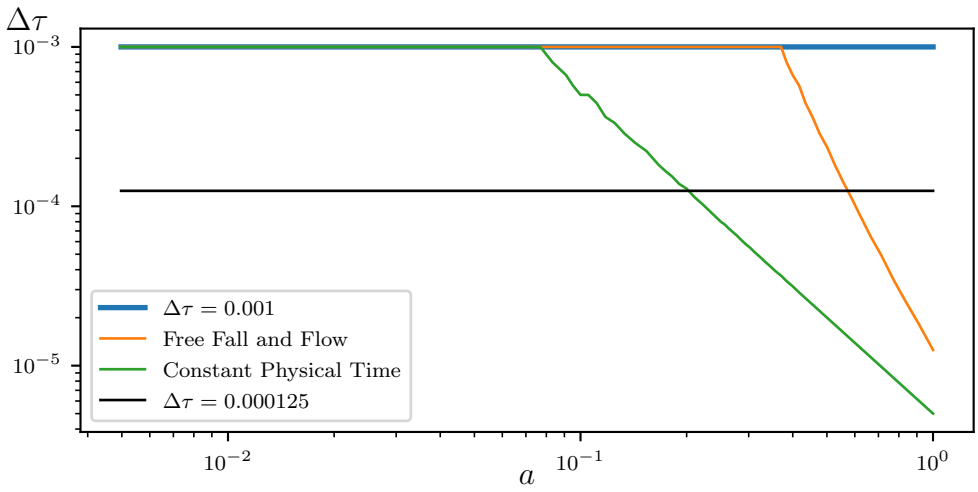

Figure 3.3: Evolution of the different dynamic time steps. Note that the CPT scale follows the power law $\propto a^{-2}$. The combined time scale of freefall time and flow time scale follows a relation closer to $\propto a^{-4}$.

0.000125 used to compute the reference wave function. We can, however, see that using an adaptive time step is a promising avenue to increase numerical accuracy, even if the different time scales must be carefully chosen in order to anticipate and prevent the sharp drop in accuracy the static time step experiences at the onset of the non-linear growth regime.

Another observation of of note is that directly after the onset of both dynamic time scales, the local Schödinger test registers a temporary loss of accuracy before an improvement is seen. It is possible that the change in time step upsets the numerical scheme such that accuracy is indeed lost for a transition period. It may also be that this is due to a larger error assigned to time step sizes in that particular interval by the test as it also indicates the reference time step of $\Delta\tau = 0.000125$ to possess a larger error. It may be possible to discern which of these is true by modifying the dynamic time step such that $\Delta\tau$ changes more gradually during the transition from static to dynamic time scales.

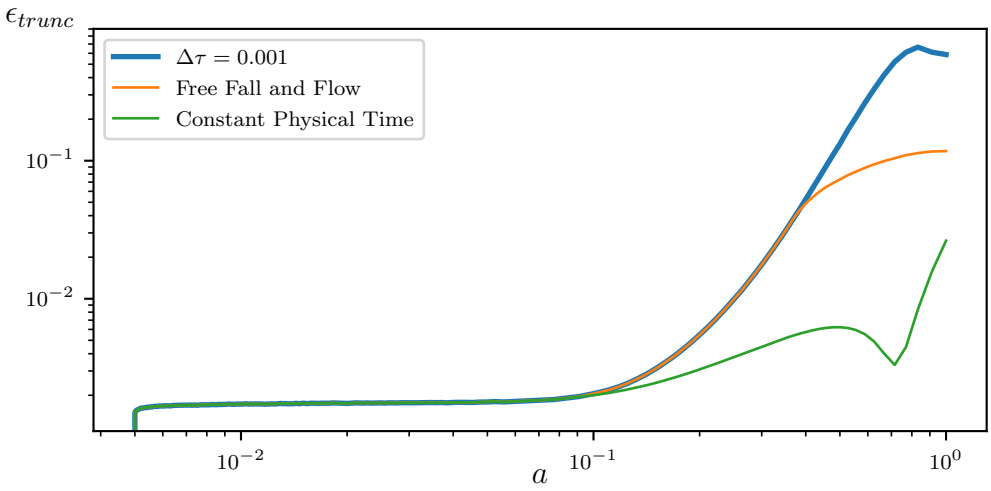

(a) Truncation error

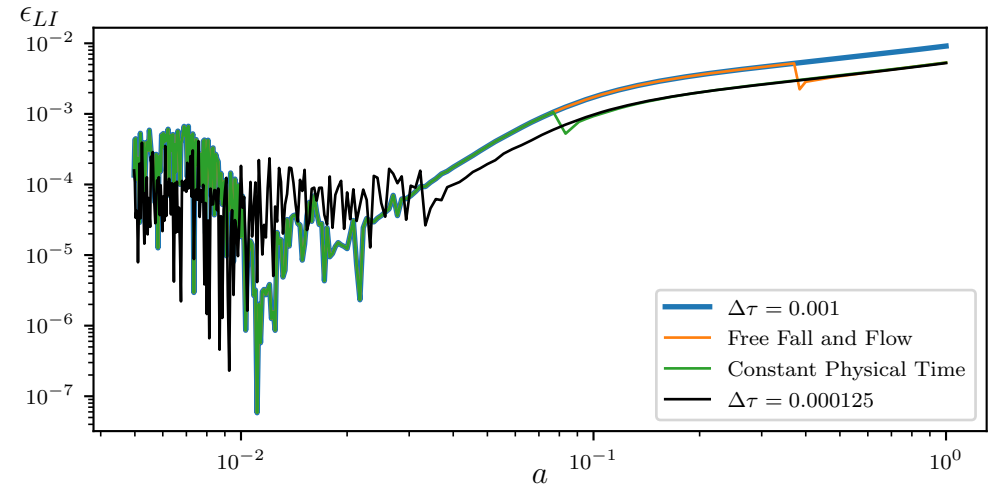

(b) Layzer-Irvine test

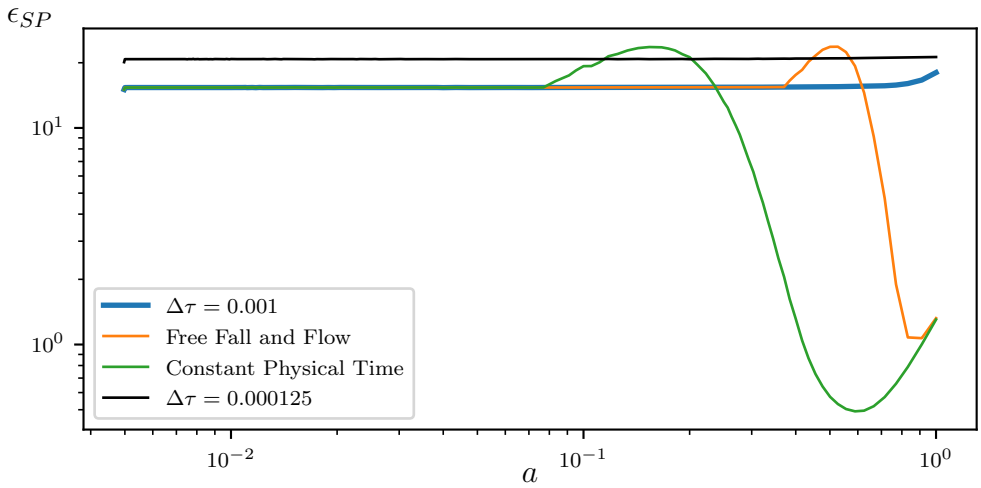

(c) Local Schrödinger test

Figure 3.4: Results for the different numerical tests for simulations using a dynamic time step. Note that the graphs overlap due to using the same time step as long as the dynamic time scales are larger than the static time step $\Delta\tau = 0.001$. Again, the Layzer-Irvine test shows little sensitivity to, e.g. the changing time steps.

Chapter 4

Conclusion

The tests we performed indicate that while the solver does indeed provide good results for the linear growth regime, it may not be feasible to use it to accurately integrate the non-linear growth regime as refining the space-time mesh may not been sufficient to overcome the growing inaccuracies that occur there. While a carefully chosen dynamic time step can alleviate this problem without an unreasonable growth in computation time, this may not be enough for a large-scale simulation to remain stable throughout the full simulation time.

Of course, our results are mainly qualitative and we can see that the tests we used have limitations that must be overcome should we desire to refine our results to come to a more definite conclusion onto whether and for which parameters the SPS solver can provide accurate results.

Using the truncation error has given us perhaps the clearest results, however its main drawback is, as addressed previously, that without an existing analytic solution, we can only approximate the error for a given solution using a sufficiently more accurate reference solution that must be computed separately. This may, particularly for tests involving already very fine meshes in space or time, such as when investigating dynamic time steps, prove prohibitively expensive in terms of computational resources required.

The problem of using the Layzer-Irvine test to gauge numerical accuracy

is that as seen, even when two solutions of the same initial conditions fulfill the energy equation tested to a high degree, those solutions may still diverge from one another without this being reflected in the energy test. This insensitivity makes it difficult to use the test when tackling the problem of accuracy within the non-linear growth regime.

The local Schrödinger test is difficult to interpret since its behaviour for different N, M is somewhat counterintuitive. In particular, the averaged local error seems to grow as $\Delta\xi$ decreases, and for high spatial resolutions, said error may sometimes be smaller for larger $\Delta\tau$. Whether this mirrors the actual accuracy, which might change in an unexpected way due to higher order terms or whether this is a defect of the test is a priori not clear.

It may be possible to improve the local Schrödinger test by computing the L_2 norm of the difference between the left hand side and the right hand side of equation (1.31) instead of taking a weighted average over all points in space. Such a quantity could possibly be interpreted as an approximation of the truncation error introduced in each time step divided by the time step size $\Delta\tau$.

The simplest way of improving the data obtained and their quantitative significance in particular would of course be to take for each set of tests the average over multiple simulations using the same parameters.

Bibliography

[1] Luca Amendola. "Linear and non-linear perturbations in dark energy models". In: *Phys. Rev. D69, 103524 (2004)* (Nov. 27, 2003). DOI: 10.1103/PhysRevD.69.103524. URL: https://arxiv.org/abs/astro-ph/0311175v2.

[2] Nora Elisa Chisari and Matias Zaldarriaga. "Connection between Newtonian simulations and general relativity". In: *Phys. Rev. D 83, 123505 (2011)* (Sept. 20, 2011). DOI: 10.1103/PhysRevD.83.123505. URL: https://arxiv.org/abs/1101.3555v3.

[3] Planck Collaboration. "Planck 2015 results. XIII. Cosmological parameters". In: *A&A 594, A13 (2016)* (Feb. 5, 2015). DOI: 10.1051/0004-6361/201525830. URL: https://arxiv.org/abs/1502.01589.

[4] Michael Kopp, Kyriakos Vattis, and Constantinos Skordis. "Solving the Vlasov equation in two spatial dimensions with the Schrödinger method". In: *Phys. Rev. D 96, 123532 (2017)* (Oct. 31, 2017). DOI: 10.1103/PhysRevD.96.123532. URL: https://arxiv.org/abs/1711.00140.

[5] David Layzer. "A Preface to Cosmogony. I. The Energy Equation and the Virial Theorem for Cosmic Distributions". In: *Ap. J. 138, 174 (1963)* (Dec. 29, 1962). DOI: 10.1086/147625.

[6] Bernard Schutz. *A First Course in General Relativity*. 2nd ed. Cambridge University Press, 2009. ISBN: 978-0-521-88705-2.

[7] Cora Uhlemann, Michael Kopp, and Thomas Haugg. "Schrödinger method as N-body double and UV completion of dust". In: *Phys. Rev. D 90, 023517 (2014)* (Mar. 17, 2014). DOI: 10.1103/PhysRevD.90.023517. URL: https://arxiv.org/abs/1403.5567.

[8] Tim Zimmermann. "A Simple Model for the Temporal Evolution of Cold Dark Matter". Bachelor Thesis. Ruperto-Carola-University of Heidelberg, 2018.

Acknowledgement

Lastly, I would like to briefly thank Sandro Wimberger and Luca Amendola for the vast support and help they provided during the preparation of this thesis and the preceding internship. Moreover, my thanks go to Tim Zimmerman for providing the code base of the SPS solver and being inordinately helpful even beyond that.

Erklärung

Ich versichere, dass ich diese Arbeit selbstständig verfasst und keine anderen als die angegebenen Quellen und Hilfsmittel benutzt habe.

Heidelberg, den ...,